Journal of Green Energy Research and Innovation

Detection and Determination of Short-Circuit Faulty Phases in Transmission Lines Compensated with a PV-Connected Series Static Synchronous Compensator

Mahyar Abasi, Ebrahim khanfari

Highlights

- **Design and Implementation of a Fault Phase Detection Algorithm for Transmission Lines Utilizing SSSC with Solar-Powered Energy Sources**
- **Formulation of a Fault Phase Detection Algorithm for Transmission Lines Based on Local Terminal Voltage Signal Analysis**
- **Development of a Fault Phase Detection Algorithm Leveraging Traveling Wave**

Graphical Abstract

Use your device to scan and read the article online

Citation

M. Abasi, and E. Khanfari, "Detection and Determination of Short-Circuit Faulty Phases in Transmission Lines Compensated with a PV-Connected Series Static Synchronous Compensator," *Journal of Green Energy Research and Innovation*, vol. 2, no. 4, pp. 67-85, 2025.

https://doi.org/10.61882/jgeri.2.4.67

CC BY NC

Journal of Green Energy Research and Innovation 2.4 (2025) 67-85

Online ISSN: 3041-9018

Journal of Green Energy Research and Innovation

Journal Homepage: www.jgeri.araku.ac.ir

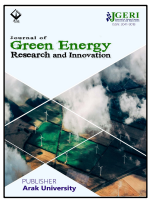

Detection and Determination of Short-Circuit Faulty Phases in Transmission Lines Compensated with a PV-Connected Series Static Synchronous Compensator

Mahyar Abasi [1,2,*], Ebrahim khanfari [3]

[1] *Department of Electrical Engineering, Faculty of Engineering, Arak University, Arak 38156-8-8349, Iran.*

[2] *Research Institute of Renewable Energy, Arak University, Arak 38156-8-8349, Iran.*

[3] *Department of Electrical and ICT, Faculty of Technical Engineering, Institute for Higher Education, ACECR, Khouzestan, Iran.*

A R T I C L E I N F O

Keywords:
Fault Detection and Classification,
Series Static Synchronous Compensator (SSSC),
Wavelet Transform in Power Systems,
Renewable Energy Systems,
Photovoltaic (PV) Integration.

Article History:
Received: 02 July 2025;
Revised: 02 August 2025;
Accepted: 05 September 2025.

Article type:
Research Article

* ***Corresponding author***
E-mail address
m-abasi@araku.ac.ir (M.Abbasi)

A B S T R A C T

Fault detection and classification in transmission lines equipped with Flexible Alternating Current Transmission System (FACTS) devices is one of the basic challenges in line protection. In the event of a fault on one side of this equipment, relays installed at the other terminal often struggle to detect the fault and determine the faulty phases due to control system interruptions in the line. The Series Static Synchronous Compensator (SSSC) is a series-connected device in transmission lines that addresses reactive power control challenges in the network. This study proposes a highly accurate and fast algorithm to detect and classify various short-circuit faults in transmission lines compensated with an SSSC. Crucially, the SSSC in this study is connected via its DC link to a solar photovoltaic (PV) farm, specifically utilizing Trina Solar Vertex N 210R-N-66 panels, allowing it to act as both a reactive power compensator and a means to seamlessly integrate this significant source of green energy into the grid. This integration highlights the method's relevance to modern renewable energy systems, particularly in enhancing the protection and monitoring of solar-powered infrastructures. The algorithm analyzes voltage signals from one side of the line, employing a discrete wavelet transform and a decision-making algorithm. The proposed method was simulated and implemented for at least 4000 fault scenarios under normal and critical conditions. Based on the extensive fault scenarios and reported results, the algorithm's performance accuracy is estimated to be approximately 98%, demonstrating its potential in improving the reliability and performance of smart and green power systems.

1. Introduction

1.1. Research motivation

One of the challenges that the electricity industry is facing today is the increasing consumption of electrical energy and the inherent lack of capacity in transmission lines. Solving the problem of line congestion and maximizing the capacity of transmission and sub-transmission lines are always the main focus of experts in the electricity sector [1]. Various solutions, such as the construction of new lines, double or multi-circuit lines, transferring power generation closer to demand centers, implementing load management at the distribution level, or the use of reactive power compensators, have been proposed. While each method offers technical advantages, they often come with their own technical or even economic disadvantages. A harmonized approach has consistently been sought to tackle this fundamental challenge. One of the plans that has attracted significant attention globally, especially in widespread countries, is the utilization of Flexible Alternating Current Transmission Systems (FACTS) devices, which are new-generation reactive power compensators. The adoption of this type of compensator in the power system assists in compensating reactive power of the load on a wide level, releasing line capacity, and increasing the active power transmission bandwidth in the lines, which, in addition to this, are very effective in dynamic and stability issues [1-3].

Furthermore, in the contemporary energy landscape, the imperative to transition towards sustainable and green energy sources has become paramount. Solar photovoltaic (PV) energy, with its abundance and environmental benefits, is a key component of this transition. Integrating large-scale solar farms into existing grid infrastructure, however, presents unique challenges, including voltage stability, power quality, and protection coordination. FACTS devices offer a promising solution by providing the necessary control and flexibility to seamlessly integrate such renewable energy sources. This integration is crucial for reducing carbon emissions, enhancing energy independence, and mitigating the impacts of climate change.

However, a significant challenge with these compensation schemes lies in the protection of transmission lines. The presence of these compensators virtually alters line parameters, rendering traditional distance relay designs ineffective in such topologies; therefore, designing protection algorithms for this type of structure is one of the critical study challenges in this field. Amongst the most prominent FACTS devices, considered a primary reactive power compensator in transmission lines, is the Series Static Synchronous Compensator (SSSC). When an SSSC is installed in the transmission line, the exact time of fault occurrence and the type of faulty phases might be misinterpreted in this topology. This is because of the very impactful dynamics of the SSSC at the time of short-circuit fault occurrence [1]. In this study, we specifically consider an SSSC whose DC link is connected to a solar farm, allowing for bi-directional power flow and enhanced grid support from renewable energy sources. This configuration adds another layer of complexity to fault detection and classification, but also offers significant advantages in terms of grid modernization and sustainability. Thus, according to the issues raised, the main challenge considered here is to address the problem of short-circuit fault detection and classification in SSSC-compensated transmission lines, particularly those integrated with solar power.

1.2. A review of the literature and research gaps

In general, the related studies and research conducted can be categorized into three basic groups based on series compensators in transmission lines. The problem considered in these three categories of issues is the discrimination of faults and non-fault conditions, and the identification of faulty phases in the transmission lines with these compensators. There are three basic categories of series compensators installed in the transmission system. Their division in this study is based on their technology. The first category includes the series capacitor compensator, which is fixed in the line and does not use any type of control switch. The second category is related to the thyristor-controlled series capacitor (TCSC) compensator, which belongs to the first generation of FACTS devices. In this type of compensator, control techniques are used to connect the capacitors to the circuit, but it still uses the static element of the capacitor in its structure. The third category of FACTS depends on the type of voltage source converter. The capacitor is not used in their structure, and the control operation is performed through a gate turn-off thyristor (GTO) switch and voltage source converters. The third type category is the most complete type of series compensator in the transmission line, whose degree of freedom and stability margin are much higher than the other two categories.

• In references [4-9], as the first category of studies, fault detection and classification methods in transmission lines compensated with series capacitors are presented, which are reviewed in detail in the following.

In reference [4], a method for detecting, classifying, and locating the faults in series capacitor-compensated transmission lines (SCTLs) is presented. Fault current signal analysis was adopted by using the combination of the discrete wavelet transform in the first level of samples and a machine learning technique. In reference [5], a method for detecting the type of faulty phase(s) in SCTLs is presented by relying on the training and learning method of neural networks based on measuring the current signal of one terminal. In this reference, the convolutional neural network based on least square error and least square regression with forgetting factor has been used. In reference [6], a protection method for fault identification and classification in series compensated transmission lines is introduced by considering the changes in instantaneous active and reactive powers. The measured quantities are drawn in a two-dimensional coordinate system, as a result of which the geometric location of each pair of instantaneous active and reactive power forms a P-Q loci curve. The quadrant of the plane where the curve starts is selected as a reference, and the curve structure is examined to identify the fault according to the displacement of the starting point under different fault conditions. In this study, the polarities of the extracted powers are also used to classify the fault based on a decision tree. In reference [7], a new method for detecting and classifying faulty lines in double-circuit SCTLs is presented by analyzing the current signals of a terminal and using the energy content of the traveling wave arriving at the terminal. The proposed method in this reference has a good performance in detecting and classifying single-circuit and intra-circuit faults in this topology. Reference [8] suggests an approach to classifying the faulty phases in high-voltage SCTLs, where the current signal of one cycle from the terminals of one side of the line is investigated based on multi-resolution wavelet analysis and a support vector machine with different feature vectors. In reference [9], a method for determining faulty phases in SCTLs based on wavelet packet transform is presented. In this method, the db10 wavelet package is used to analyze the waveform of the faulty phase current to obtain the wavelet energy coefficients.

• As the second category of studies, in references [10-18], fault detection and classification methods in TCSC-compensated transmission lines are presented, which are reviewed in detail below.

In reference [10], a method based on the combination of minimal radial basis function neural networks and fuzzy neural networks is presented for classifying and locating the faults in lines compensated with TCSC. This requires the smallest number of neurons, fewer fuzzy rules, and less processing. In reference [11], a new approach based on a decision tree is presented to find the faulty area and categorize the faulty lines in the transmission lines compensated with TCSC and using the current signals of one terminal and zero-sequence voltage. In reference [12], a method for fault location and faulty line identification in transmission lines with a TCSC is discussed. The method uses the current signals of one terminal for the input of a binary and multi-class support vector machine solver. In reference [13], a method is introduced by adopting the support vector machine to recognize the type of fault in TCSC-compensated transmission lines. The approach uses three-phase half-cycle current samples for fault detection. In reference [14], based on the superimposed energy method, a fault identification and categorization in TCSC-compensated transmission lines is

provided. In this reference, energy polarity analysis is used to identify fault occurrence within the zone and outside the zone. In reference [15], mathematical morphology is utilized to detect and classify faults in TCSC-compensated transmission lines. The method adopts the features of simplified mathematical morphology to analyze the current signals of a terminal in the transmission line. In reference [16], a fault detection and classification method for transmission lines with a TCSC linked to a wind farm is presented. The theory uses the distance relay comprehensive protection scheme based on the fuzzy characteristic curve in an adaptive way. The method is robust against fault resistance. In reference [17], a fault classification method in transmission lines with a TCSC is presented using the fault current analysis and support vector machine classifier method. The latter is very resistant to the saturation of current transformers and the presence of noise. In reference [18], a fault detection method during power fluctuation in transmission lines with a TCSC is provided based on three-phase current measurements of one terminal. The solution incorporates a decision tree to solve the mentioned challenge. In the following, in references [19-24], as the third category of studies, fault detection and classification methods in SSSC-compensated transmission lines are presented, which are reviewed in detail below.

In reference [19], a fault classification technique in transmission lines with an SSSC is introduced. It depends on the entropy technique combined with the wavelet in the time-frequency domain to analyze the current and voltage signals during the fault. In reference [20], a comprehensive distance protection scheme using the wavelet packet entropy analysis is used to solve the challenge of correctly detecting the faulty area in SSSC-compensated transmission lines. In this design, the frequency resolution has been improved at high-frequency levels. In reference [21], a fault detection and classification scheme in transmission lines with an SSSC is presented with relying on wavelet transform and regression trees. In this design, both the advantages of the resolution characteristic of the wavelet transform and Shannon entropy are used in the description of the signal characteristics and as the input of the decision tree. In reference [22], a fault detection and location scheme in SSSC-compensated transmission lines is discussed based on traveling wave theory. The method uses the wavelet transform and modal transform to analyze current and voltage signals. The main focus of this plan is to prevent the low-frequency interference created by the system when a fault occurs on the left and right sides of the SSSC. In reference [23], a pilot distance protection method is presented to enhance the distance relay's performance in case of faults in SSSC-compensated transmission lines. The design can be implemented adaptively by digital relaying algorithms. In reference [24], an ultra-fast protection method based on wavelet transform is presented for internal and external fault discrimination in transmission lines with an SSSC by incorporating storage components. The design is resistant to the operation state of the compensator, and there is no need to utilize adaptive designs.

Based on a comprehensive analysis of the existing literature cited in this study ([1]– [20]), we have identified several critical research gaps that directly motivate and justify the contributions of the proposed method. These are summarized below**:**

1. Dependency on Current Signals and Dual-Terminal Measurements **:**Many previous works ([1], [3], [6], [12], [14]) rely on both voltage and current measurements, and some even require synchronized dual-terminal data. These approaches are vulnerable to CT saturation, require expensive infrastructure, and are impractical in weakly monitored or rural lines **.**

- ❖ Our method uses only single-terminal voltage, thus reducing cost, improving reliability, and simplifying deployment**.**

2. Lack of Realistic Modeling for FACTS Devices Integrated with Renewables: While FACTS-based protection methods are explored (e.g., [5], [8], [10]), most assume idealized models of SSSC and neglect the complexity introduced by PV integration. The nonlinear dynamics of SSSC operation with a photovoltaic DC source are often not considered.

- ❖ Our model includes a realistic PV-fed SSSC with dynamic interaction, reflecting real-world control behavior and voltage support characteristics.

3. Generic or Arbitrary Use of Wavelet Transforms **:**Prior wavelet-based techniques ([2], [11], [13]) often select decomposition levels arbitrarily and fail to justify the use of specific mother wavelets. Some focus on higher levels (e.g., CD4–CD6), ignoring the high-frequency transients essential for fast detection.

- ❖ We use db6 with 9 levels and focus on CD1, which was empirically validated to be the most responsive to fault-induced disturbances.

4. Limited Fault Scenarios and Lack of Stress Testing: Many methods are validated only under ideal or limited operating conditions, with few works testing under high-resistance faults, noise, load fluctuations, or power oscillations ([4], [9], [15]).

- ❖ We conducted over 4000 simulations, including 7 critical scenarios involving high-impedance faults, dynamic SSSC modes, zero-crossings, noise, and no-fault disturbances**.**

5. No Integration with PV Source Behavior in Protection Logic: Very few works consider the impact of PV intermittency and power injection patterns on fault detection performance**.**

- ❖ Our method maintains detection accuracy despite transient power variability from the PV-connected SSSC, which is critical for smart grid deployment.

6. Threshold Selection Lacks Statistical Justification: Several studies use static thresholds or heuristics without quantitative calibration ([3], [10], [13]).

- ❖ We employ a data-driven threshold strategy using a wavelet-energy-based statistical analysis derived from a comprehensive dataset of simulated events.

7. Absence of Real-World Implementation Considerations**:** Some AI- or ML-based methods ([16], [17], [18]) are difficult to implement in real-time due to black-box behavior or excessive computational cost.

- ❖ The suggested method is simple, interpretable, and suitable for relay-level implementation without complex hardware dependencies.

These gaps directly shape the foundation of our proposed algorithm. We have designed the method to address real-world protection challenges in PV-integrated SSSC environments using a robust, scalable, and computationally efficient voltage-based wavelet technique. This ensures practical feasibility and scientific innovation aligned with the modern requirements of smart and renewable-rich power systems**.**

1.3. Novelty and contribution

The present study provides a high-performance approach to fault detection and classification in transmission lines compensated with an SSSC, specifically focusing on scenarios where the SSSC's DC link is connected to a solar photovoltaic (PV) farm utilizing Trina Solar Vertex N 210R-N-66 panels. This configuration is increasingly vital for integrating clean and green energy sources into the grid, but it also introduces complexities in grid protection. The proposed method uniquely utilizes only the three-phase voltages from one terminal on the fault side, enhancing its practicality and cost-effectiveness for such critical infrastructure. The measured voltage signals transform into a set of coefficients, specifically one approximate and nine detail coefficients, using the discrete wavelet transform with the db6 mother wavelet and a decomposition level of 9. The detail coefficient of level 1 from all three phases, combined with a decision tree-based process and predetermined threshold values proportional to the network under study and derived from the Otsu method, is effectively employed for robustly detecting and classifying various short-circuit faults, including Single-Line-to-Ground (SLG), Line-to-Line-to-Ground (LLG), Line-to-Line (LL), and Three-Phase (LLL) faults, on both sides of the SSSC. The technique was meticulously programmed in the MATLAB software environment and rigorously analyzed and evaluated across numerous normal and critical scenarios, including those reflecting the dynamic behavior associated with solar farm integration. The reported results consistently confirm the algorithm's highly acceptable performance, demonstrating its potential to significantly enhance the reliability of modern power grids relying on renewable energy.

The key innovations of this paper are presented below:

1. Design and implementation of a faulty phase detection algorithm for transmission lines utilizing SSSC with solar-powered energy sources.
2. Formulation of a faulty phase detection algorithm for transmission lines based on local terminal voltage signal analysis.
3. Development of a faulty phase detection algorithm leveraging traveling wave characteristics and wavelet transform techniques.
4. Establishment of a faulty phase detection algorithm independent of fault section identification in relation to SSSC.

1.4. Paper organization

The remaining sections of the paper are introduced here. Section 2 provides the methodology, the suggested algorithm, and the complete flowchart of the problem. Section 3 reports the results of implementing the algorithm in the software platform. Section 4 describes the sensitivity analysis reports of the algorithm. The conclusions and a summary of the paper are given in Section 5.

2. The proposed method

2.1. Structure of the network under study

The test network is introduced in a general way. According to Figure 1, the network considered in this paper consists of two Thevenin's equivalent circuits, which are considered main networks and are interconnected via a transmission line between terminals T_1 and T_2. In this structure, a dynamic load that is a reactive power consumer is connected to terminal T_2. An SSSC is located in the middle of the line to compensate for reactive power and also to control dynamic load fluctuations. In the current study, three-phase voltages measured at terminal T_1 are sampled by a transducer with a sampling frequency of 10 kHz and are provided to the algorithm for fault detection and classification.

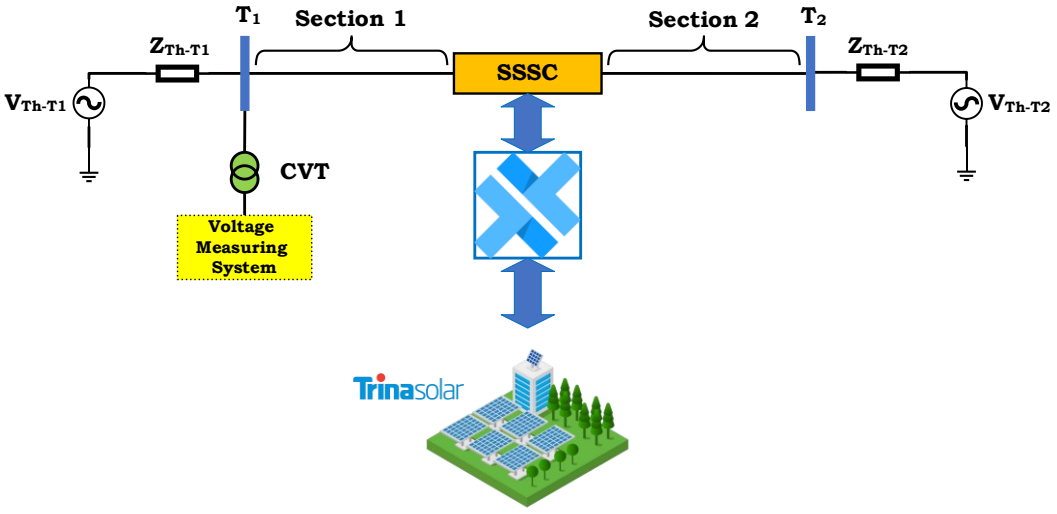

Figure 1. Single-line diagram of the test system.

2.2. Formulation

This subsection presents the formulation of the problem. Discrete Wavelet Transform (DWT) is utilized to establish the proposed algorithm. By analyzing the three-phase voltage signal at different levels, extracting accurate and approximate coefficients from low-pass and high-pass filters, and designing a comparison algorithm based on an innovative decision tree, a method for detecting the faulty phase(s) has been presented. In the following, the theory of DWT is presented first, and then the proposed method to solve the challenge of classifying the faulty phases in a topology compensated with SSSC will be presented.

2.2.1. DWT theory

Wavelet theory was proposed a few decades ago for the analysis of non-stationary signals. Due to its oscillating characteristic, the wavelet provides the conditions to perform a time-frequency analysis of the signal. Similar to the Fourier transform, the wavelet of a signal can be expanded based on the mother and daughter wavelets. Wavelet functions are obtained from a function called the mother wavelet, and these functions are called daughter wavelets. Each daughter wavelet is created by scaling and shifting the mother wavelet. Like the Fourier series, if we consider c_j as wavelet coefficients and $w_j(x)$ as the mother wavelet set, the function $f(x)$ is expanded in the form of Equation (1).

$$f(x) = \sum_{j=0}^{m} c_{jw_j}(x) \tag{1}$$

In Equation (1), $m+1$ is the total number of coefficients and $M = 2^m - 1$ is the number of levels in the wavelet transform. Finally, after applying the wavelet functions at different levels, $f(x)$ can be expanded in the form of Equation (2).

$$f(x) = c_0\varphi(x) + \sum_{i=0}^{\infty}\sum_{k=0}^{2^i-1} c_{2^i+k} w(2^i x - k) \tag{2}$$

where, $\varphi(x)$ is called the scale function. Theoretically, the wavelet transform of a signal can be continued up to infinity, but the number of wavelet transform levels depends on the type of analysis and the need we have to extract different frequencies from the signal. So, in Equation (2), the upper limit of parameter i is set to the number M, which is the last level required for the wavelet transform. Suppose we expand the function f(x) at the $(j+1)$ th level using only the scale functions $\varphi_{j+k}(x)$, where j is the number of the level and k is the position of the scale function. The coefficients that express the relationship between the function $f(x)$ and the function $f(x)$ can be represented by a, which is taken from the word "approximation", as given in Equation (3).

$$f(x) = a_1\varphi(x) + a_2\varphi(2x) + a_3\varphi(2x-1) + \ldots \tag{3}$$

which are obtained from Equation (4) by considering the orthogonality condition of the scaling functions of coefficients a.

$$a_{j+1}(k) = 2^{j+1}\int f(x)\varphi(2^{j+1}x - k)dx \tag{4}$$

Finally, having a coefficient, f(x) is written as Equation (5):

$$f(x) = \sum_k a_{j+1}(k)\varphi(2^{j+1}x - k) \tag{5}$$

Now, with a lower level, i.e., up to the jth level, if we expand the function f(x) mentioned in Equation (6) using scale functions and wavelet functions, the coefficients obtained from wavelet functions are shown by the letter d, which is derived from the word “detail”.

$$f(x) = \sum_k a_j(k)\varphi(2^j x - k) + \sum_k d_j(k) w(2^j x - k) \tag{6}$$

where, $a_j(k)$ and $d_j(k)$ can be described using Equations (7) and (8).

$$a_j(k) = 2^j \int f(x)\varphi(2^j x - k)dx \tag{7}$$

$$d_j(k) = 2^j \int f(x) w(2^j x - k)dx \tag{8}$$

By inserting the scale function $\varphi(x)$ and the wavelet function $w(x)$, Equations (7) and (8) will become as Equations (9) and (10), respectively [25].

$$a_j(k) = 2^j \int f(x) \langle \sum_n g_0(n)\varphi(2(2^j x - k) - n)\rangle dx \tag{9}$$

$$d_j(k) = 2^j \int f(x) \langle \sum_n g_1(n)\varphi(2(2^{j+1}x - 2k) - n)\rangle dx \tag{10}$$

By swapping integral and sum operators, Equation (9) can be expanded first as Equation (11) and finally as Equation (12).

$$a_j(k) = 2^j \sum_n g_0(n) \int f(x)\varphi(2^{j+1}x - 2k - n)dx \tag{11}$$

And if $2k + n = m$, then we have Equation (12):

$$a_j(k) = \sum g_0(m - 2k) 2^j \int f(x)\varphi(2^{j+1}x - m)dx \tag{12}$$

And finally, after equating, Equation (12) can be expanded as Equation (13), where $h_0(n)$ are coefficients of the decomposer high-pass filter.

$$a_j(k) = \frac{1}{2}\sum g_0(m - 2k) a_{j+1}(m) = \sum_m h_0(2k - m) a_{j+1}(m) \tag{13}$$

And if we write the same equations for Equation (10), finally, we can reach Equation (14) without providing intermediate relations. where $h_1(n)$ are coefficients of the decomposer high-pass filter.

$$d_j(k) = \frac{1}{2}\sum g_1(m - 2k) a_{j+1}(m) = \sum h_1(2k - m) a_{j+1}(m) \tag{14}$$

Equations (13) and (14) are the main relations of the discrete wavelet transform. These two equations state that every discrete data set can be divided into two categories. The first category is the details that are obtained by passing the information through a high-pass filter, and the second category is the estimate that is obtained by passing the information through a low-pass filter.

In Equations (13) and (14), a concept called decimation is used. In the literal sense, decimation means choosing one object from among 10 objects, but in the above equations, it means choosing one among the numbers output from the filters. This action is also called down-sampling. The opposite of decimation is the act of interpolation, that is, placing one number between two other numbers. This concept is used in the reconstruction of signals whose wavelet coefficients are available. According to the concept expressed in the wavelet transform, M in the discrete wavelet transform is 2 [26,27]. In other words, the relationship between input ($x(n)$) and output ($y(n)$) is as follows:

$$y(n) = x(2n) \tag{15}$$

Finally, the basic structure of the discrete wavelet transform can be shown in Figure 2:

In Figure 1, u_d(k) and u_a(k) are obtained from Equations (16) and (17):

$$u_d(\mathrm{k}) = \sum \mathrm{h}_1(\mathrm{k}-\mathrm{n})\mathrm{a}_{\mathrm{j}+1}(\mathrm{n}) \tag{16}$$

$$\mathrm{u}_\mathrm{a}(\mathrm{k}) = \sum \mathrm{h}_0(\mathrm{k}-\mathrm{n})\mathrm{a}_{\mathrm{j}+1}(\mathrm{n}) \tag{17}$$

With decimation, Equations (16) and (17) can be written as Equations (18) and (19).

$$\mathrm{d}_\mathrm{j}(\mathrm{k}) = \sum \mathrm{h}_1(2\mathrm{k}-\mathrm{n})\mathrm{a}_{\mathrm{j}+1}(\mathrm{n}) = \sum \mathrm{h}_1(\mathrm{n})\mathrm{a}_{\mathrm{j}+1}(2\mathrm{k}-\mathrm{n}) \tag{18}$$

$$\mathrm{a}_j(\mathrm{k}) = \sum \mathrm{h}_0(2\mathrm{k}-\mathrm{n})\mathrm{a}_{\mathrm{j}+1}(\mathrm{n}) = \sum \mathrm{h}_0(\mathrm{n})\mathrm{a}_{\mathrm{j}+1}(2\mathrm{k}-\mathrm{n}) \tag{19}$$

If we decompose an arbitrary signal with the coefficients of the decomposing filter ($h_0(n)$ and $h_1(n)$) by using the coefficients of the reconstruction filters ($g_0(n)$ and $g_1(n)$), the original signal will be re-established. If signal $f(k)$ is a discrete function, its wavelet transform can be described in the form of Equations (20) and (21), where $d(k)$ represents the coefficients of the wavelet transform of signal f at the first level, and other numbers obtained from the signal decomposition are an estimate of the signal.

$$d(k) = \sum_{n=0}^{N-1} h_1(2k-n)f(n) = \sum_{n=0}^{N-1} h_1(n)f(2k-n) \tag{20}$$

$$a(k) = \sum_{n=0}^{N-1} h_0(2k-n)f(n) = \sum_{n=0}^{N-1} h_0(n)f(2k-n) \tag{21}$$

In this paper, to analyze the three-phase signal measured from terminal T_1, level 9 wavelet signal analysis is used. The selection of level 9 for wavelet decomposition was made based on extensive testing under various fault conditions. In over 4000 simulated fault scenarios—including SLG, LLG, LL, and LLL faults—level 9 decomposition using the db6 mother wavelet provided the most consistent and discriminative CD1 coefficients across all three phases. Higher decomposition levels enable better isolation of the high-frequency transients generated by different fault types, especially those masked by the dynamic behavior of the SSSC and the intermittent output of the connected PV system. Lower levels (e.g., 4 to 7) resulted in insufficient frequency resolution, causing overlap between fault and non-fault events, while levels above 9 increased computations without noticeable performance gain. Thus, level 9 offered an optimal trade-off between resolution and efficiency, ensuring precise classification of faulted phases with minimal complexity. This empirical tuning was a key step in maximizing the detection accuracy of the proposed method. After extracting CD_9 from the voltage of all three phases and using a decision tree-based plan depending on the threshold values, it is possible to detect a fault and categorize the faulty phases. Figure 3 shows the decomposition diagram of a signal into estimated and detailed coefficients in level 9. The selection of this level for the analysis of the raised problem was done by trial and error and experimentally in the implementation of different fault scenarios. At this level, the algorithm's performance is the best performance state with the least error [28].

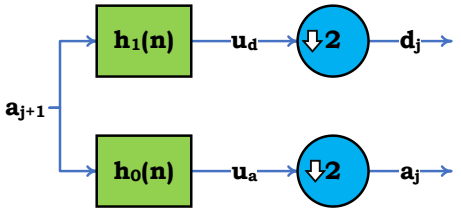

Figure 2. Signal decomposition into two levels.

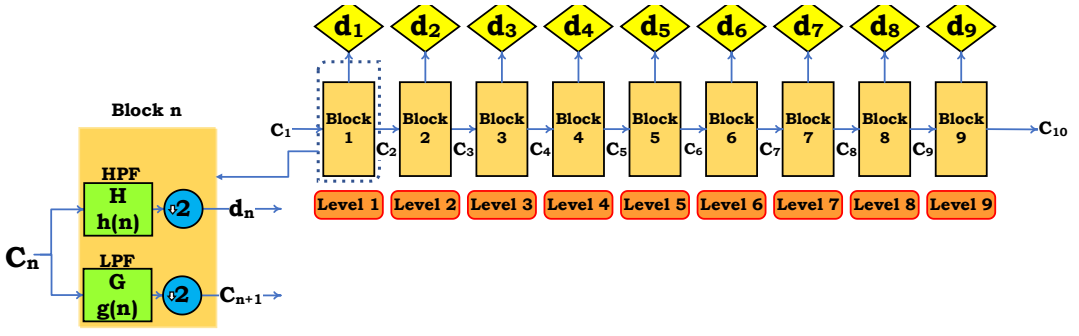

Figure 3. Diagram of decomposing signal into nine levels.

2.2.2. Describing the logic of the proposed algorithm

In this subsection, the aim is to present the logic of the algorithm according to the results of applying the wavelet transform on the three-phase voltage signal. This study exclusively uses three-phase bus voltage signals at terminal T_1 for fault detection and classification. This choice is deliberate and offers practical benefits. Voltage signals are more stable and reliable than current signals, especially under severe fault conditions where current transformers (CTs) may saturate and distort measurements. Voltage transformers (VTs), on the other hand, are less affected by such distortions. Additionally, using only voltage reduces sensor requirements, simplifies implementation, and lowers costs—making the method well-suited for real-world applications, particularly in smart grids with integrated renewable energy. It also ensures robust performance by minimizing the influence of current variations caused by load changes or PV power fluctuations. Overall, this design enhances reliability and is considered one of the key strengths of the proposed method. According to the results of the coefficients extracted from the wavelet transform used for the three-phase voltage signal, the fault detection and classification algorithm is defined as follows in different parts. The theory presented uses three threshold values, namely, Thr0, Thr1, and Thr2, whose values are obtained in a per-unit system based on the implementation of at least 4000 scenarios. In the simulation section, the numerical values of these thresholds are given according to the network under study.

***A**. Fault detection*

At this level, it must first be determined whether a fault has occurred at all or not. To implement this problem, the maximum value of the detail coefficient 1 (MAX_CD1) can be used. If MAX_CD1 exceeds Thr0 for even one of the phases (a, b, c), then a fault must have occurred. The reason is that if at least one phase is involved in a fault, then high-frequency fluctuations of that phase will be higher than the predetermined threshold value, and a fault must have appeared. If there is no fault, CD1 in a pre-unit system is almost zero, but when a fault occurs, the high-frequency fluctuations of the voltage of that phase increase, so in this case, a fault must have happened, but its type is not clear at this stage.

***B**. Ground fault detection*

If the value of MAX_CD1 of two phases is greater than Thr1 (the threshold value), or MAX_CD1 of all three phases is less than Thr2, then no ground fault has occurred; otherwise, if one of the rules is rejected when a non-grounded fault occurs, the high-frequency oscillation behavior of at least two phases relative to the other phase increases from the threshold value of Thr1, which is several times greater than Thr2. If it is a grounded fault, MAX_CD1 will never increase from the Thr3 because some of the fault energy is damped through the ground, which causes high-frequency oscillations in the faulty phases in at least one of the faulty phases smaller than Thr1. Also, if the MAX_CD1 values of all three phases are smaller than Thr2, then it is a non-ground fault that can cover the three-phase state. Otherwise, a ground fault must have occurred.

***C**. Faulty phase(s) detection*

This case itself is divided into two parts, which will be discussed separately in the following.

Case 1: The fault is phase-to-phase. In this case, if the MAX_CD1 of two phases is greater than the threshold value of Thr1, it means that the fault must have occurred in those two phases; otherwise, the fault is a three-phase type.

Case 2: The fault is in the form of phase(s) to ground. In this case, the fault occurs either as LG or LLG. If the fault is LG, the MAX_CD1 of that phase will be higher than the other two phases, and also the MAX_CD1 of the other two phases will be lower than Thr2. However, in the case the fault is LLG, then MAX_CD1 of the faulty two phases will be higher than MAX_CD1 of the non-fault phase, and at the same time, MAX_CD1 of the faulty phases becomes larger than Thr2; otherwise, the fault is a LLLG.

The threshold values Thr0, Thr1, and Thr2 used in the proposed fault classification algorithm were derived through a rigorous multi-stage process involving signal processing, empirical analysis, and classification validation. These thresholds serve as discriminators to identify faulty phases under various fault types by evaluating the behavior of voltage waveforms using wavelet-based energy signatures. The voltage signals at terminal T_1 were processed using the discrete wavelet transform (DWT) with the db6 mother wavelet at decomposition level 9. This setup was chosen to capture transient components localized in the high-frequency range — typically caused by abrupt impedance discontinuities during fault inception. Among all decomposition levels, detail level 1 (CD1) was found to be the most sensitive and consistent in revealing fault-related variations across different phases. To calibrate the thresholds, we simulated over 4000 fault scenarios encompassing:

- All major fault types (SLG, LL, LLG, LLL),
- Wide fault resistance variation (1–100 Ω),
- Different inception angles and times (6.5–9 s),
- Both left-side and right-side positions with respect to the SSSC.

For each scenario, the CD1 energy peak of each phase was recorded, normalized, and categorized. Using statistical methods inspired by Otsu-based clustering, the optimal thresholds were selected such that intra-class variance (between faulty and non-faulty phase energy levels) was minimized. Threshold Thr0 acts as the primary activation level, distinguishing between faulty and healthy phases. Thr1 and Thr2 serve as secondary criteria to refine fault classification in the presence of overlapping waveform energies, particularly under low-resistance or remote faults where waveform energy is less pronounced. The derived thresholds are thus specific to the signal dynamics of the test system, shaped by the SSSC's real-time compensation behavior and the intermittency of the PV source. This tuning strategy enhances faulty phase identification accuracy and reduces misclassification in complex operating environments.

2.3. Pseudo-code of the proposed algorithm

In this part, the general program related to the proposed algorithm is given in several levels in Figure 4.

```
START
Stage 1. Calling the three-phase voltage signal of the terminal
    Vt=Vabc.Signals. values';
Stage 2. Run the wavelet transform
wpt = wpdec(P,9,'db6');
cfs = abs (wpcoef(wpt,[9 0]));
    For Level=1 to 9
wpt = wpdec(P,9,'db6');
cfs = abs (wpcoef(wpt,[ Level 1]));
    End
Stage 3. Fault detection and classification
    3.1. Determining threshold values, calculating peak values , and defining error flags
    3.2. Fault detection unit
            For all phases
                    If peak values are greater than the threshold value
                            Fault Flag = 1
                    Else
                            Fault Flag = 0
            End
    3.3. Ground fault detection unit
            If Fault Flag = 1
                    For all phases
    If PeakVal of two phases is greater than Thr1 OR Three of PeakVal are less than Thr2
Ground Flag = 0
    Else
                            Ground Flag = 1
            End
                    End
             Else
                    Display "No Fault"
            End
    3.4. Phase-to-phase fault detection unit
            If Ground Flag = 1
                    For all phases
    If PeakVal of two phases is greater than Thr1
Phase-to-phase fault detected in these two phases
    Else
                            Three-phase faults
            End
                    End
             End
    3.5. phase(s) to the ground fault detection unit
            If Ground Flag = 1
                    For all phases
    If PeakVal of one phase is greater than PeakVal of two phases
    AND
       PeakVal of two phases Less than Thr2
            One phase to ground fault
    Else if PeakVal of one phase is less than PeakVal of two phases
        AND
          PeakVal of two phases Greater than Thr2
            Two-phase-to-ground fault
            End
                    End
             End
END
```

Figure 4. Pseudo-code of the proposed algorithm.

3. Software simulation and results analysis

3.1. Normal operation

Now we introduce the network under study in the MATLAB/Simulink software. According to Figure 5, this network includes two main grids with a 500 kV voltage level and 1400 MVA power, which feed a dynamic load with a power of 220 MVA through a 100 km line. The complete information of this network for implementation in the MATLAB/Simulink software is given in Table 1. Since the reactive power demand of the dynamic load is assumed very high in this network, an SSSC based on a power oscillation damper (POD) has been adopted to provide this reactive power and also to control the desired load. According to the intended goals, the considered SSSC is located in the middle of the 100 km line. Under fault-free conditions, the performance of the network under study in the presence of SSSC has been investigated in terms of compensating for the reactive power demanded by the load. The considered dynamic load consumes 0.8 p.u. amount of reactive power. In this simulation, the moment the SSSC is switched to the network is considered 5 seconds after the start of the simulation. The reference value of vq is set at 0.05 p.u. After switching on the SSSC, a part of the reactive power demanded by the dynamic load is supplied through the SSSC, and the reactive power output of the connected networks in both terminals is reduced. Figure 6 displays the three-phase voltage and current measured from two terminals on both sides of the fault. Also, according to Figure 7, the reactive power demand of the load, reactive power injected by the SSSC, and reactive power produced by the networks connected to the terminals are measured in this case. Figure 7 shows that when the SSSC switches on the circuit at the moment $t = 5$ s, the SSSC injects reactive power equivalent to 1 p.u. into the transmission line. Concurrently, the power consumption of the load has not changed, but this injected power compensates for a part of the reactive power demand of the load, and for this reason, the production power of networks 1 and 2 decreases. Moreover, to examine the performance of the SSSC control system, the reference and actual values of vq followed by the POD controller are plotted in Figure 8. As it is observed, at $t = 5$ s that the SSSC is switched on, q-axis voltage follows the reference value with high accuracy and injects part of the reactive power demand of the load into the network. Figure 8 also demonstrates that the SSSC controller can follow the reference value of 0.05 p.u. with high accuracy and thus inject the predicted reactive power into the network. By increasing the power ratio of SSSC, compensation can be done in such a way that all the power demand of the dynamic load is fed by the compensator, and the reactive power produced by the main grids reaches zero.

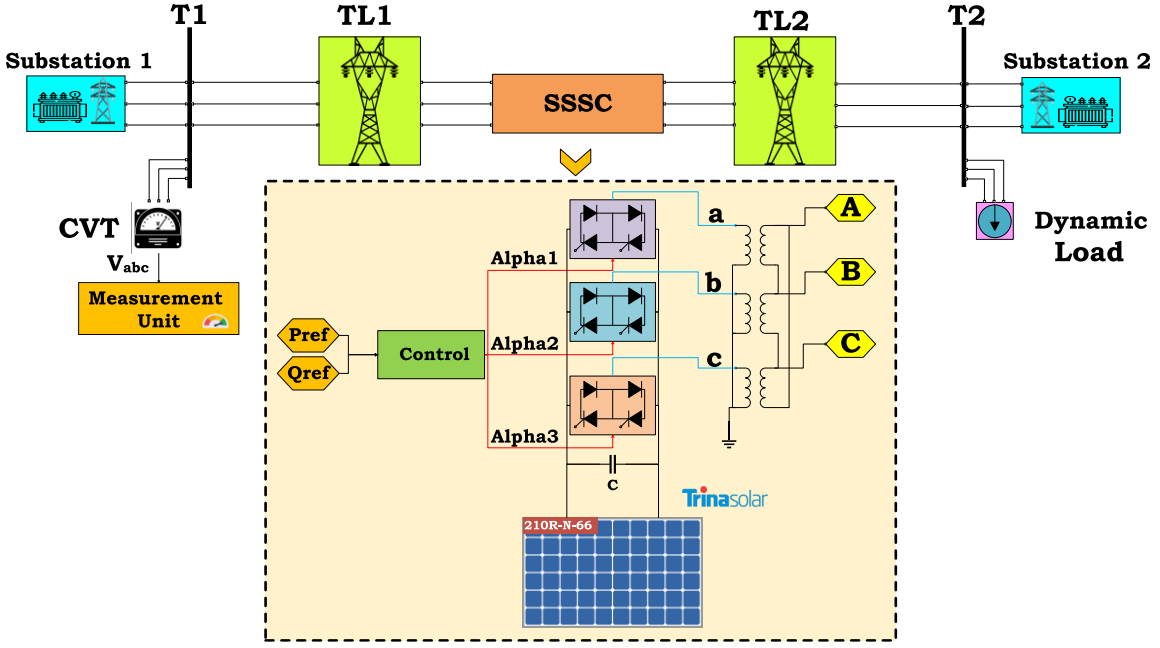

Figure 5. Three-phase diagram of the test network in MATLAB simulation environment.

Table 1. Data of the test network for MATLAB simulation.

Line parameters	Value
Positive-sequence resistance (R1) (Ω/km)	0.02546
Zero-sequence resistance (R0) (Ω/km)	0.3864
Positive-sequence inductance (L1) (H/km)	0.00093
Zero-sequence inductance (L0) (H/km)	0.0041264
Positive-sequence capacitance (C1) (H/km)	$1.27 \times 10\text{-}8$
Zero-sequence capacitance (C0) (H/km)	$7.751 \times 10\text{-}9$
Length of the line segment (km)	50
Line frequency (Hz)	50
Synchronous generator parameters	**Value**
Rated voltage (kV)	13.8
Xd (p.u.)	1.305
Xd' (p.u.)	0.296

Xd" (p.u.)	0.252
Xq (p.u.)	0.474
Xq" (p.u.)	0.243
Xl (p.u.)	0.18
Frequency of power sources (Hz)	50
Td' (s)	1.01
Td" (s)	0.053
Tq0" (s)	0.1
Rs	0.0028544
H (s)	3.7
Pair of poles	32
Initial angle (deg)	-58.9841
Initial current of phases a, b, c (p.u.)	0.763417
Initial angle of phase a (deg)	14.3746
Initial angle of phase b (deg)	-105.625
Initial angle of phase c (deg)	134.375
Excitation voltage (p.u.)	1.2256
Parameters of generators' three-phase transformers	Value
Rated power (MVA)	2100
Frequency (Hz)	50
Primary voltage (kV)	13.8
Secondary voltage (kV)	500
R1 (p.u.)	0.002
L1 (p.u.)	0
R2 (p.u.)	0.002
L2 (p.u.)	0.12
Rm (p.u.)	500
Lm (p.u.)	500
Connection type	Star-delta
Characteristics of the dynamic load	Value
Rated voltage (kV)	500
Rated frequency (Hz)	50
Active power (W)	2.2×109
Reactive power (Var)	0.8×108
Primary positive-sequence voltage (p.u.)	1.00208
Primary positive-sequence angle (deg)	20.9514
Characteristics of the SSSC	Value
Rated voltage (kV)	500
Rated frequency (Hz)	50
Rated power of the series converter (MVA)	100
Injected voltage (p.u.)	0.1
R (p.u.)	0.00533
L (p.u.)	0.16
DC-link voltage (V)	40000
DC-link capacitance (F)	0.000375
Trina Solar- 210R-N-66	Value
Module power (W)	700
Module Efficiency (%)	22.5
ISC (A)	17.44
VOC(V)	49.4
Maximum Power Voltage-VMPP (V)	43.2
Maximum Power Current-IMPP (A)	9.96
NOCT (Nominal Operating Cell Temperature)	43
Max Series Fuse Rating (A)	25

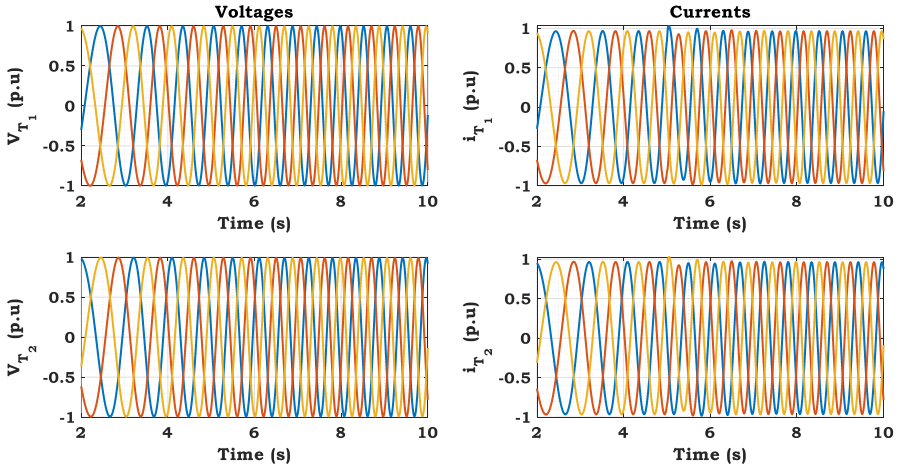

Figure 6. Three-phase voltages measured on terminals T_1 and T_2 of the transmission line.

3.2. Fault scenarios and results analysis

In this part, the goal is to evaluate the algorithm in different fault scenarios in the transmission line compensated with SSSC. According to the network modeled in Figure 5 and also the pseudocode of the algorithm in Figure 4, the threshold values of this network are equal to 0.05, 1.7, and 0.6, respectively. These threshold values have been obtained in a per-unit system based on the implementation of at least 4000 fault scenarios. To evaluate the proposed algorithm, the three-phase voltages of terminal T_1, as well as the threshold values, are needed. In the following, five scenarios are used to test the proposed algorithm. These scenarios have been implemented for different points of the line on both sides of the SSSC, as well as for different resistance values and different phases. According to the results presented in the implementation of the scenarios, the algorithm's performance is assessed as very favorable.

Scenario 1: In this scenario, an AG fault appears 80 km away from terminal T_1 with R = 10 Ω at t = 7 s. The three-phase voltage diagram of terminal T_1 in the time domain is given in Figure 9. After measuring this voltage and applying DWT and extracting CD1 according to Figure 10 for all three phases and measuring the maximum values of this detail coefficient and comparing them with the threshold values and with each other, according to the flowchart in Figure 4, the implementation result is given in Figure 11, where the performance of the proposed algorithm is evaluated as very favorable.

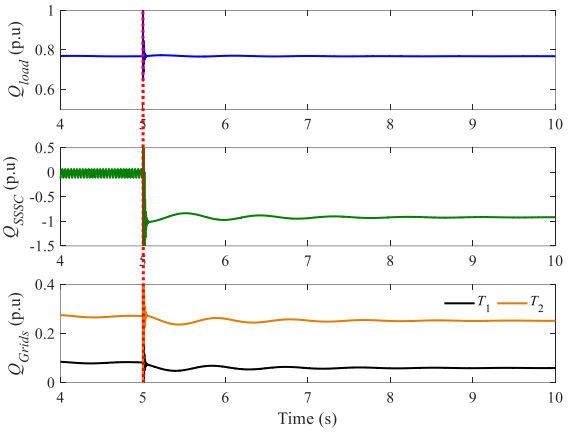

Figure 7. The reactive power demand of the dynamic load, the reactive power injected by SSSC on Terminal 2, and the reactive power generated by the networks connected to Terminals 1 and 2.

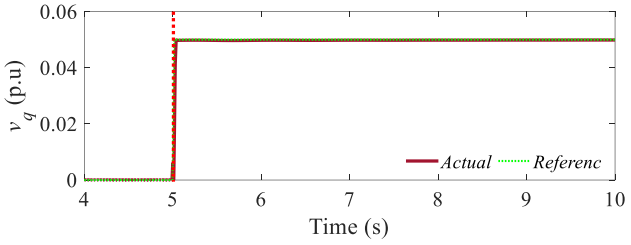

Figure 8. Real and reference v_a values tracked by the POD controller.

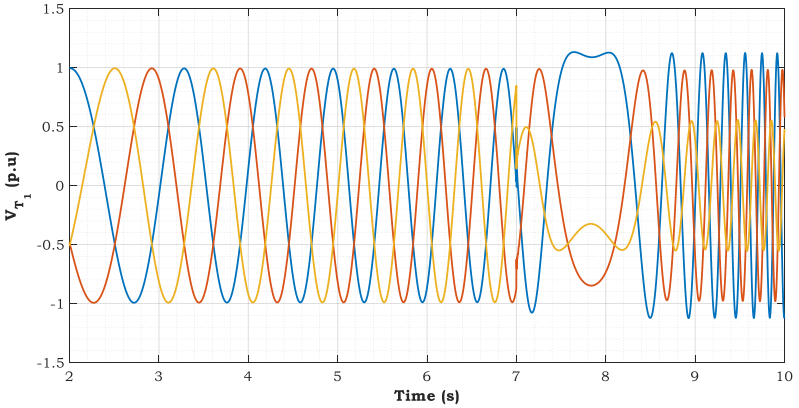

Figure 9. Three-phase voltage of terminal T_1 in accordance with the implementation of Scenario 1.

Scenario 2: In this scenario, an AG fault appears 30 km away from terminal T_1 with R = 10 Ω at t = 8 s. The three-phase voltage diagram of terminal T_1 in the time domain is given in Figure 12. After measuring this voltage and applying DWT and extracting CD1 according to Figure 13 for all three phases and measuring the maximum values of this detail coefficient and comparing them with the threshold values and with each other according to the flowchart in Figure 4, the result of implementation is shown in Figure 14, where the performance of the proposed algorithm is evaluated as very favorable.

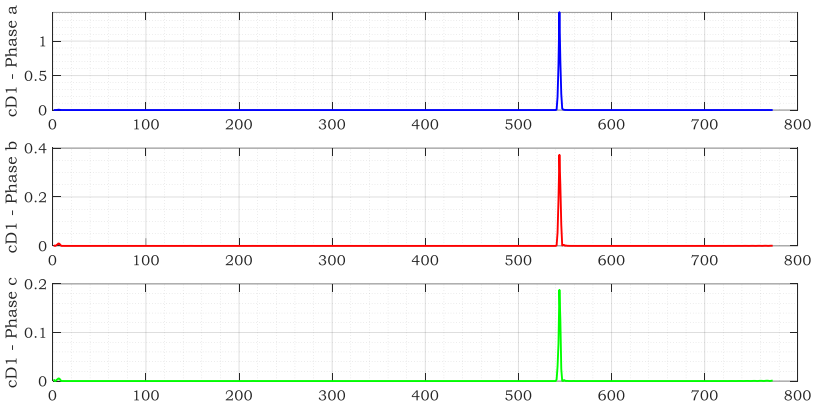

Figure 10. Detail coefficients of level 1 of all three phases a, b, and c, corresponding to the three-phase voltage of Terminal T_1 in Scenario 1.

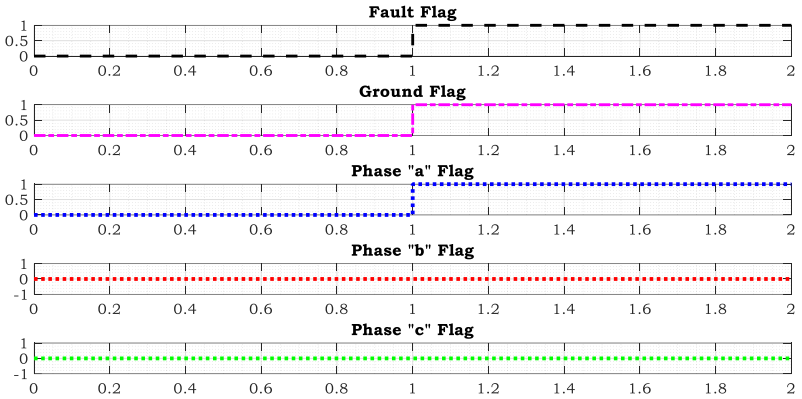

Figure 11. The performance results of the algorithm in detecting a fault, detecting whether the fault is grounded or not, and detecting the faulty phases in Scenario 1.

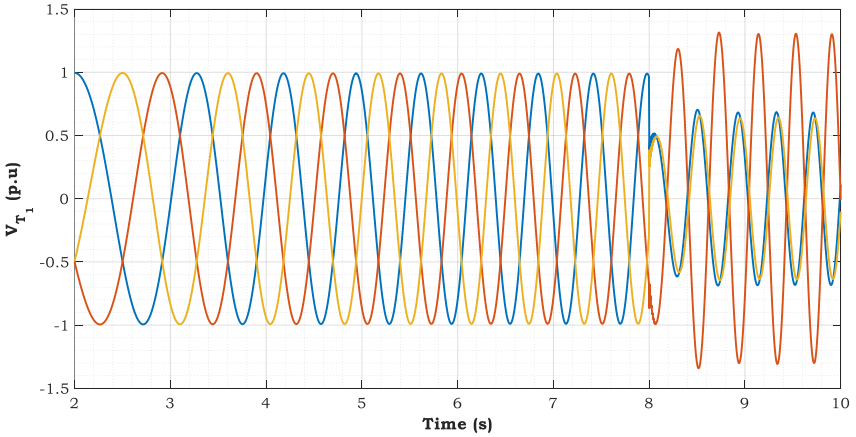

Figure 12. Three-phase voltage of terminal T_1 according to the implementation of scenario 2.

Scenario 3: In this scenario, an ABG fault occurs at 55 km away from terminal T_1 with R = 50 Ω at t = 6.5 s. The three-phase voltage diagram of terminal T_1 in the time domain is given in Figure 15. After measuring this voltage and applying DWT and extracting CD1 according to Figure 16 for all three phases and measuring the maximum values of this detail coefficient and comparing them with the threshold values and with each other according to the pseudocode of Figure 4, the result of the implementation is depicted in Figure 17, where the algorithm's performance is evaluated as very favorable.

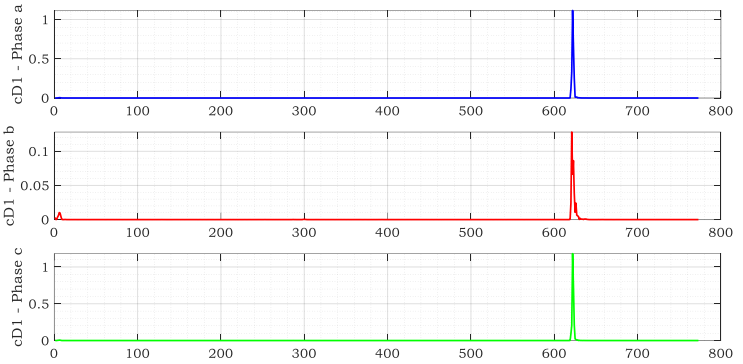

Figure 13. Detail coefficients of level 1 of all three phases a, b, and c, corresponding to the three-phase voltage of terminal T_1 in scenario 2.

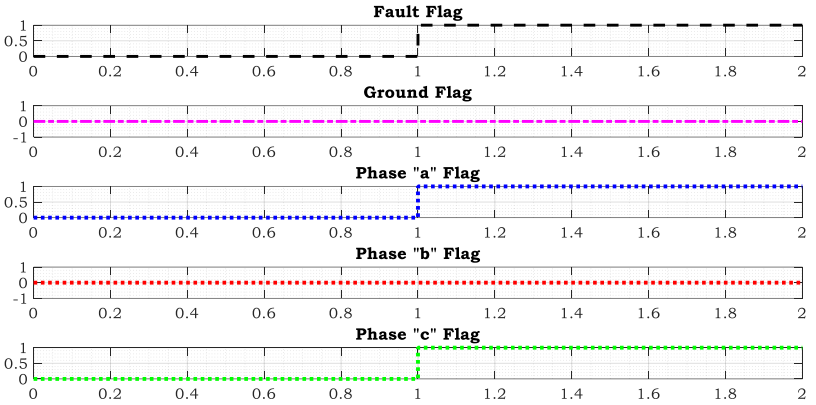

Figure 14. The performance results of the algorithm in detecting a fault, detecting whether the fault is grounded or not, and detecting the faulty phases in scenario 2.

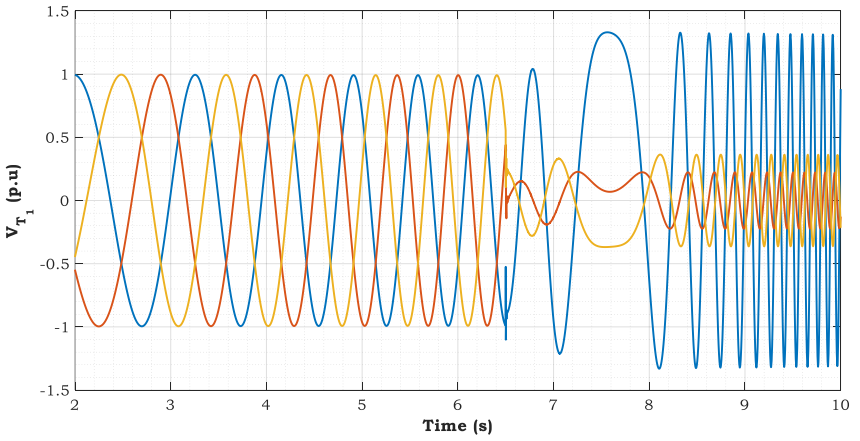

Figure 15. Three-phase voltage of terminal T_1 according to the implementation of scenario 3.

Scenario 4: In this scenario, an ABC fault appears 20 km away from terminal T_1 with R = 1 Ω at t = 8 s. The three-phase voltage diagram of terminal T_1 in the time domain is given in Figure 18. After measuring this voltage and applying DWT and extracting CD1 according to Figure 19 for all three phases and measuring the maximum values of this detail coefficient and comparing them with the threshold values and with each other according to the flowchart in Figure 4, the result of implementation is provided in Figure 20, where the algorithm's performance is evaluated as very favorable.

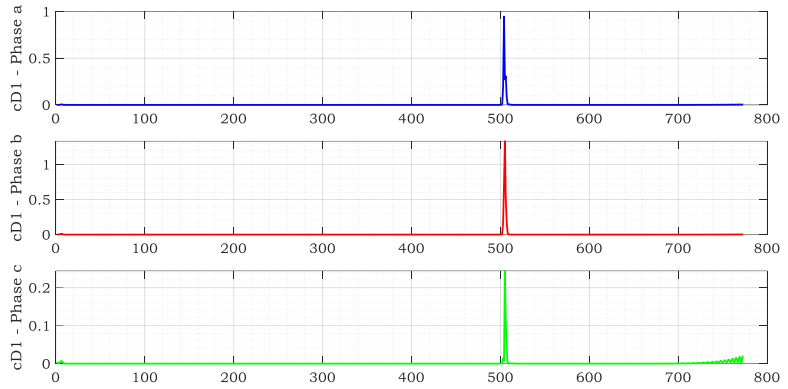

Figure 16. Detail coefficients of level 1 of all three phases a, b, and c, corresponding to the three-phase voltage of terminal T_1 in scenario 3.

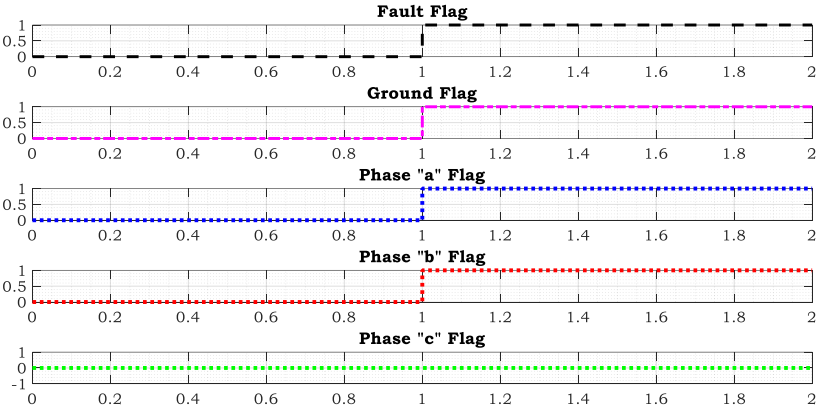

Figure 17. The performance results of the algorithm in detecting a fault, detecting whether the fault is grounded or not, and detecting the faulty phases in scenario 3.

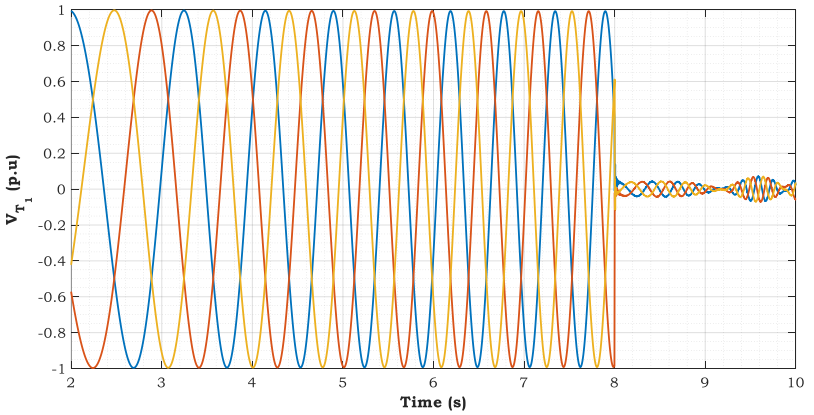

Figure 18. Three-phase voltage of terminal T_1 according to the implementation of scenario 4.

Scenario 5: In this scenario, a CG fault appears 65 km away from terminal T_1 with R = 100 Ω at t = 9 s. The three-phase voltage diagram of terminal T_1 in the time domain is given in Figure 21. After measuring this voltage and applying DWT and extracting CD1 according to Figure 22 for all three phases and measuring the maximum values of this detail coefficient and comparing them with the threshold values and also comparing them with each other according to the pseudocode of Figure 4, the result of the implementation is illustrated in Figure 23, where the algorithm's performance is evaluated as very favorable.

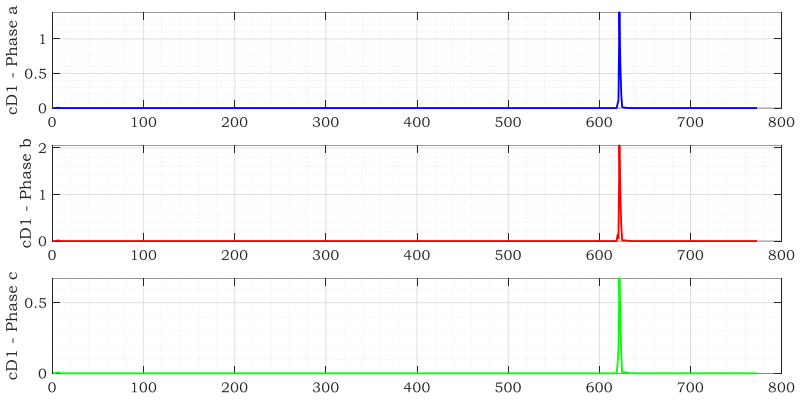

Figure 19. Detail coefficients of level 1 of all three phases a, b, and c, corresponding to the three-phase voltage of terminal T_1 in Scenario 4.

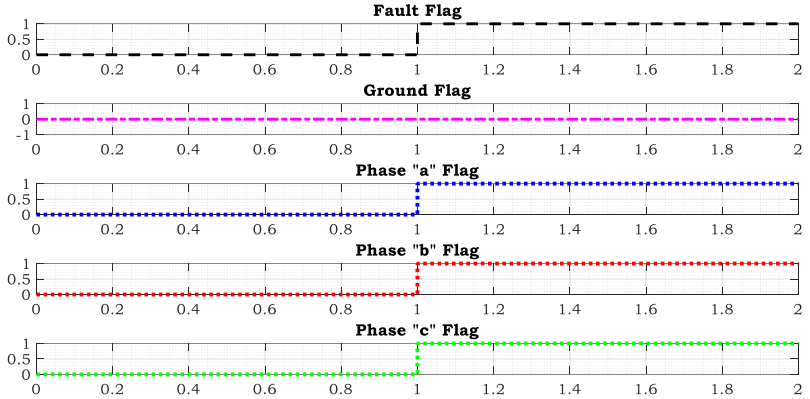

Figure 20. The performance results of the algorithm in detecting a fault, detecting whether the fault is grounded or not, and detecting the faulty phases in Scenario 4.

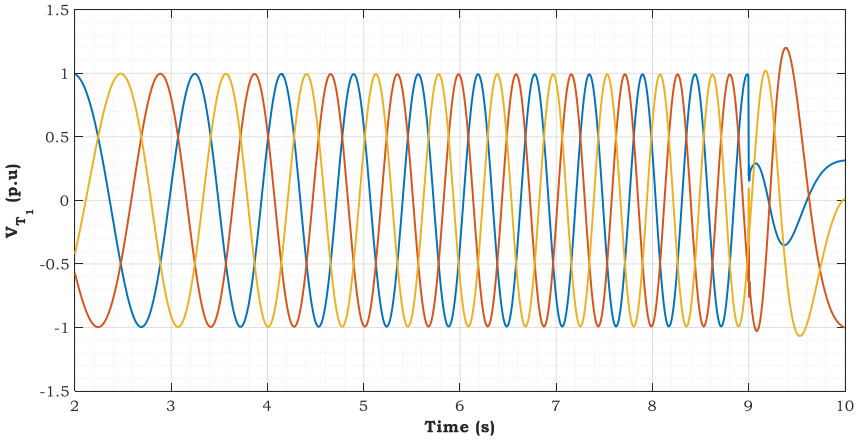

Figure 21. Three-phase voltage of terminal T_1 according to the implementation of Scenario 5.

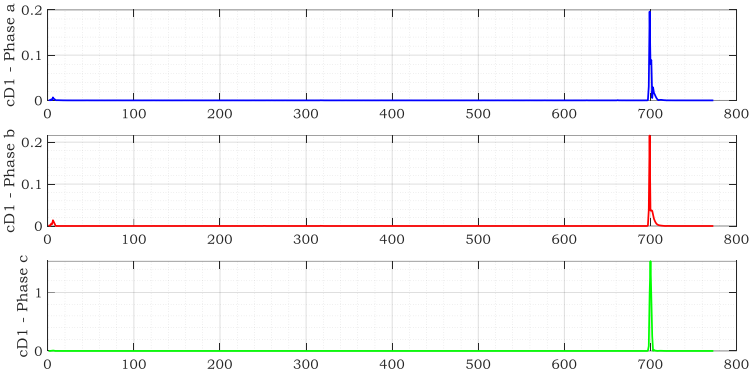

Figure 22. Detail coefficients of level 1 of all three phases a, b, and c corresponding to the three-phase voltage of terminal T_1 in Scenario 5.

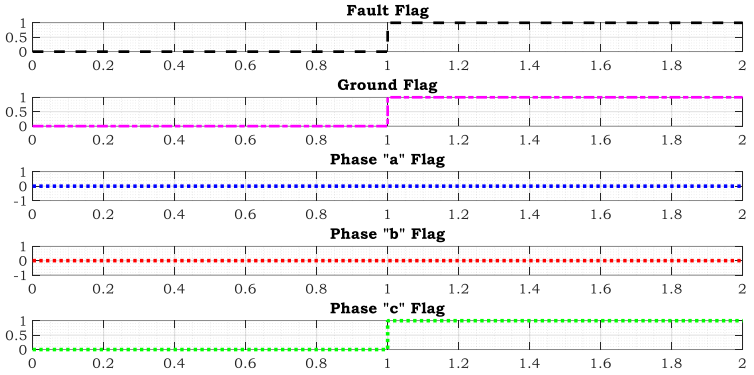

Figure 23. The performance results of the algorithm in detecting a fault, detecting whether the fault is grounded or not, and detecting the faulty phases in Scenario 5.

4. Sensitivity analysis of the proposed algorithm

The goal here is to evaluate the proposed algorithm with respect to seven critical scenarios. According to the results obtained in Section 3, the algorithm's performance during a fault is very favorable in normal conditions. Nonetheless, now we evaluate the algorithm's performance for very critical conditions. Here, the resistance of the algorithm to critical conditions has been tested and evaluated.

Scenario 1 sensitivity analysis: In this sensitivity analysis, the SSSC is assumed to be placed 25% closer to terminal T_2. An AB fault occurred 90 km away from terminal T_1 at $t = 6$ s with a resistance of 20 Ω. The implementation results of this scenario are tabulated in Table 2 in the row related to SA1. According to the obtained results, the algorithm is not sensitive to the location of SSSC and works correctly.

Scenario 2 sensitivity analysis: In this sensitivity analysis, a BCG fault is assumed at 60 km away from terminal T_1 with a fault resistance value of 250 Ω at $t = 5.5$ s. The implementation results are provided in Table 2 in the row related to SA2. According to the obtained results, the suggested algorithm is a little sensitive to the high-resistance fault. The final value of this resistance is 317 Ω at and the fault occurs at 95 km away from terminal T_1 and is a single-phase to ground fault.

Scenario 3 sensitivity analysis: In this sensitivity analysis, an AG fault appears at 40 km away from terminal T_1 with a phase-to-phase resistance of 3 Ω when phase A voltage of terminal T_1 crosses the zero point. The implementation results are shown in Table 2 in the row related to SA3. According to the obtained results, it is shown that the proposed algorithm is resistant to crossing the zero-voltage point.

Scenario 4 sensitivity analysis: In this sensitivity analysis, a power oscillation is assumed with a frequency deviation of 1 Hz in the generator connected to terminal T_2 for 3 cycles before a solid AB fault occurrence at 55 km away from terminal T_1 at $t = 6$ s. The fault occurred during power oscillation. The implementation results are presented in Table 2 in the row related to SA4. According to the obtained results, the algorithm is resistant to power oscillations due to the use of POD.

Scenario 5 sensitivity analysis: In this sensitivity analysis, the dynamic fluctuations of the load connected to terminal T_2 will increase by 20% in terms of active power (this process is done by increasing the angle and frequency). In this case, no fault has occurred in the network. The implementation results are presented in Table 2 in row SA5. According to the presented results, the suggested algorithm successfully detects the absence of a fault and has not detected this phenomenon as a fault. As shown, the algorithm is resistant to critical conditions similar to faults.

Scenario 6 sensitivity analysis: In this sensitivity analysis, the operation mode of SSSC is changed. In this case, the reference value has changed from 0.5 to 0.1 p.u. In this situation, a CG fault occurred 75 km away from terminal T_1 at $t = 7$ s with R = 50 Ω. The implementation results are tabulated in Table 2 in row SA6. According to the results, the algorithm is resistant to changing the learning mode of SSSC, so the proposed design can be implemented in any operation mode.

Scenario 7 sensitivity analysis: In this sensitivity analysis, a white Gaussian noise of 20 dB is injected into the voltage measurement of bus T_2 for 3 cycles before the fault. In this case, an AB fault appears at 80 km away from terminal T_1 with R = 10 Ω. The value of 20 dB considered in this case is the critical limit of injection noise, in which case the algorithm works correctly; otherwise, the performance of the algorithm will be disturbed by increasing the value of this level of noise. The implementation results are provided in Table 2 in row SA7. According to the presented results, the performance of the algorithm in these critical limit conditions is acceptable.

The conducted sensitivity analysis rigorously evaluates the algorithm's performance under extreme grid conditions that frequently challenge conventional protection schemes. Each of the seven scenarios targets a distinct vulnerability in real-world transmission systems compensated by FACTS devices and exposed to renewable integration. These include:

- High-impedance faults (SA2, SA6): where signal attenuation tests the algorithm's capacity to distinguish low-energy transients.
- Zero-voltage crossing conditions (SA3): This challenges the time-frequency resolution of CD1 features.
- Pre-fault power oscillations (SA4): This introduces false harmonic content, potentially masking true fault signatures.
- Non-fault dynamic load shifts (SA5): Validating the algorithm's immunity to operational disturbances.
- Controller setpoint variation in the SSSC (SA6): This alters the voltage regulation regime and affects waveform morphology.
- Gaussian noise in VT measurements (SA7): pushing the threshold margins to their detection limits.

Across all scenarios, the proposed threshold-based decision logic—grounded in energy analysis of level-1 wavelet coefficients (CD1)—demonstrates consistent phase selectivity and fault-type discrimination. The statistical dispersion of CD1 peak values across faulted and non-faulted phases remained within designed bounds (Thr0, Thr1, Thr2), ensuring high robustness even under distorted, delayed, or weakened signal conditions. This sensitivity validation confirms that the threshold values are not only empirically optimized but "electrodynamically grounded", accounting for the nonlinearities introduced by SSSC control behavior, PV intermittency, and measurement imperfections. The algorithm's resilience to these multidimensional disturbances substantiates its suitability for deployment in complex modern grids.

5. Conclusion

This paper developed and validated a novel, high-performance algorithm for detecting and classifying short-circuit faults in SSSC-compensated transmission lines, using only single-terminal voltage measurements. The method is rooted in a signal processing approach that exploits the high time-frequency localization properties of the DWT. By employing the db6 wavelet function and decomposing the voltage signals up to level 9, the algorithm captures subtle high-frequency transients associated with fault inception. Among all decomposition levels, the first-level detail coefficients (CD1) consistently exhibited the highest sensitivity to abrupt disturbances, making them ideal for fault signature extraction. A rigorous feature extraction mechanism based on CD1 peak energy across phases was established, followed by a multi-threshold decision algorithm utilizing three empirically calibrated thresholds (Thr0, Thr1, Thr2). These thresholds effectively separated faulty from healthy phases under complex system conditions. To ensure robustness, the method was evaluated across more than 4000 fault scenarios, covering:

- All conventional fault types (SLG, LL, LLG, LLL),
- Fault resistances ranging from 1 to 317 Ω,
- Different locations relative to the SSSC (both left and right sides),
- Variable fault inception times (6.5–9.0 s),
- Phase-dependent zero-crossing conditions.

In addition to normal scenarios, seven critical operating conditions were simulated, such as:

- SSSC control reference variation, altering the line's reactive compensation dynamics,
- Gaussian white noise (20 dB) added to voltage signals,
- Pre-fault power oscillations that distort the voltage waveform spectrum,
- Dynamic load changes, mimicking active disturbances in practical systems.

Table 2. The results of the implementation of different sensitivity analysis scenarios.

Scenario No.	Maximum values of CD1 for the three phases of terminal T_1			Implementation results				
	Phase c	Phase b	Phase a	Is there a fault?	Is it a ground fault?	Which phase is faulty? Phase c	Phase b	Phase a
SA1	1.1	1.09	0.15	Yes	No			
SA2	0.25	1.4	1.01	Yes	Yes			
SA3	1.39	0.29	0.22	Yes	Yes			
SA4	1.12	0.12	1.11	Yes	No			
SA5	0.15	0.11	0.09	No	No			
SA6	0.26	0.33	1.32	Yes	Yes			
SA7	1.13	1.11	0.17	Yes	No			

Despite these challenges, the algorithm maintained a 98% accuracy rate in correctly detecting faulty phases and classifying fault types. The wavelet-based energy signatures proved resilient against noise and signal distortion, and the algorithm's independence from current measurements mitigates CT saturation and reduces implementation complexity. Unlike many prior studies, which either rely on dual-terminal data, assume ideal conditions, or ignore FACTS behavior, the proposed method explicitly accounts for the dynamic behavior of an SSSC connected to a PV source — a non-trivial integration often ignored in literature.

Proposed research directions (deep and technically grounded) include:

1. Adaptive threshold tuning using real-time disturbance metrics: Developing an online adjustment mechanism for Thr0–Thr2 based on instantaneous signal quality or system states (e.g., SSSC modulation depth or PV variability).

2. Hybrid wavelet-ML architectures: Integrating machine learning models (e.g., ensemble classifiers, GBDT, CNN) trained on wavelet-domain features to enhance classification under uncertain topologies.

3. Spatiotemporal coordination with PMU data: Extending the method to wide-area protection schemes using synchronized phasor measurements and GPS-based event correlation.

4. Real-time FPGA/RTDS implementation: Deploying the proposed method on hardware platforms to evaluate latency, resource usage, and feasibility in practical protection relays.

5. multi-objective optimization of wavelet parameters: Using evolutionary algorithms (e.g., NSGA-II) to jointly optimize wavelet type, decomposition depth, and threshold margins under noisy or uncertain environments.

6. Generalization to meshed and looped networks: Validating the method in more complex topologies where multiple FACTS or PV sources introduce nonlinear interactions in the protection zone.

References

[1] M. Abasi, M. Joorabian, A. Saffarian, and S. Seifossadat, "A Comprehensive Review of Various Fault Location Methods for Transmission Lines Compensated by FACTS Devices and Series Capacitors," *Journal of Operation and Automation in Power Engineering*, vol. 9, no. 3, pp. 213–225, 2021.

[2] M. Abasi, and O. Sadeghian, "A Ground Fault Location Algorithm in Double-circuit Transmission Lines with T-off Connection to an Industrial Microgrid by Using Current and Voltage Phasors Information of a Single Terminal," *IET Generation, Transmission & Distribution*, vol. 18, no. 8, pp. 1714–1741, 2024.

[3] M. Abasi, A. Saffarian, M. Joorabian, and S. G. Seifossadat, "Fault Location in Double-Circuit Transmission Lines Compensated by Generalized Unified Power Flow Controller (GUPFC) Based on Synchronous Current and Voltage Phasors," *IEEE Systems Journal*, vol. 15, no. 2, pp. 2190–2200, 2021.

[4] V. Malathi, N. Marimuthu, S. Baskar, and K. Ramar, "Application of Extreme Learning Machine for Series Compensated Transmission Line Protection," *Engineering Applications of Artificial Intelligence*, vol. 24, no. 5, pp. 880–887, 2011.

[5] B. Y. Vyas, B. Das, and R. P. Maheshwari, "Improved Fault Classification in Series Compensated Transmission Line: Comparative Evaluation of Chebyshev Neural Network Training Algorithms," *IEEE Transactions on Neural Networks and Learning Systems*, vol. 27, no. 8, pp. 1631–1642, 2016.

[6] J. R. Moparthi, D. P. Chinta, and S. Nakka, "Two-Dimensional Curve Variation Approach-Based Quick Fault Detection and Classification Scheme for Series Compensated Transmission Line System," *International Transactions on Electrical Energy Systems*, vol. 29, no. 3, e2738, 2018.

[7] G. Kapoor, "A Protection Technique for Series Capacitor Compensated 400 kV Double Circuit Transmission Line Based on Wavelet Transform Including Inter-Circuit and Cross-Country Faults," *International Journal of Engineering, Science and Technology*, vol. 11, no. 2, pp. 1–20, 2019.

[8] P. D. Raval, and A. S. Pandya, "A Novel Fault Classification Technique in Series Compensated Transmission Line Using Ensemble Method," *International Journal of Pattern Recognition and Artificial Intelligence*, vol. 34, no. 04, 2050009, 2019.

[9] A. R. Adly, S. H. Abdel Aleem, M. A. Elsadd, and Z. M. Ali, "Wavelet Packet Transform Applied to a Series-Compensated Line: A Novel Scheme for Fault Identification," *Measurement*, vol. 151, 107156, 2020.

[10] D. Pradhan, and Panda, "Application of Artificial Intelligence Techniques for Classification and Location of Faults on Thyristor-Controlled Series-Compensated Line," *Electric Power Components and Systems*, vol. 31, no. 3, pp. 241–260, 2003.

[11] S. Samantaray, "Decision Tree-Based Fault Zone Identification and Fault Classification in Flexible AC Transmissions-Based Transmission Line," *IET Generation, Transmission & Distribution*, vol. 3, no. 5, pp. 425–436, 2009.

[12] B. Yashvantrai Vyas, R. P. Maheshwari, and B. Das, "Pattern Recognition Application of Support Vector Machine for Fault Classification of Thyristor Controlled Series Compensated Transmission Lines," *Journal of The Institution of Engineers (India): Series B*, vol. 97, pp. 175–183, 2016.

[13] B. Yashvantrai Vyas, R. P. Maheshwari, and B. Das, "Pattern Recognition Application of Support Vector Machine for Fault Classification of Thyristor Controlled Series Compensated Transmission Lines," *Journal of The Institution of Engineers (India): Series B*, vol. 97, no. 2, pp. 175–183, 2015.

[14] O. H. Gupta, and M. Tripathy, "Superimposed Energy-Based Fault Detection and Classification Scheme for Series-Compensated Line," *Electric Power Components and Systems*, vol. 44, no. 10, pp. 1095–1110, 2016.

[15] G. Kapoor, "An SMMBG-Based Relaying Technique for Detection and Categorization of Faults in TCSC-Compensated Transmission Lines," *Journal of Electrical and Electronics Engineering*, vol. 13, no. 1, 2020.

[16] A. A. R. Mohamed, H. M. Sharaf, and D. K. Ibrahim, "Enhancing Distance Protection of Long Transmission Lines Compensated with TCSC and Connected with Wind Power," *IEEE Access*, vol. 9, pp. 46717–46730, 2021.

[17] N. H. Kothari, B. R. Bhalja, V. Pandya, and P. Tripathi, "A Rate-Of-Change-Of-Current Based Fault Classification Technique for Thyristor-Controlled Series-Compensated Transmission Lines," *International Journal of Emerging Electric Power Systems*, vol. 23, no. 3, pp. 289–304, 2021.

[18] S. Kumar Mohanty, A. Swetapadma, P. Kumar Nayak, and O. P. Malik, "Decision Tree Approach for Fault Detection in a TCSC Compensated Line During Power Swing," *International Journal of Electrical Power & Energy Systems*, vol. 146, 108758, 2023.

[19] A. M. El-Zonkoly, and H. Desouki, "Wavelet Entropy Based Algorithm for Fault Detection and Classification in FACTS Compensated Transmission Line," *Energy and Power Engineering*, vol. 03, no. 01, pp. 34–42, 2011.

[20] Q. Liu, Y. Y. Chang, and Y. Xu, "Fault Position Identification for Series Compensated Lines with SSSC Based on Improved Wavelet Packet Entropy," *Advanced Materials Research*, vol. 383-390, pp. 5200–5205, 2011.

[21] M. Geethanjali, M. A. Alias, and T. K. S. Pandy, "Discrete Wavelet Transform Based Fault Detection and Classification in a Static Synchronous Series Compensated Transmission System," *Advances in Intelligent Systems and Computing*, pp. 85–94, 2014.

[22] E. Reyes-Archundia, J. L. Guardado, E. L. Moreno-Goytia, J. A. Gutierrez-Gnecchi, and F. Martinez-Cardenas, "Fault Detection and Localization in Transmission Lines with a Static Synchronous Series Compensator," *Advances in Electrical and Computer Engineering*, vol. 15, no. 3, pp. 17–22, 2015.

[23] M. M. Almomani and S. F. Algharaibeh, "Modelling and Testing of a Numerical Pilot Distance Relay for Compensated Transmission Lines," International Journal of Scientific Research and Engineering Development, vol. 3, no. 6, 2020.

[24] H. V. Gururaja Rao, N. Prabhu, and R. C. Mala, "Wavelet Transform-Based Protection of Transmission Line Incorporating SSSC with Energy Storage Device," *Electrical Engineering*, vol. 102, no. 3, pp. 1593–1604, 2020.

[25] H. Hanif, M. Zand, M. Azimi Nasab, S. M. S. Ghiasi, and S. Padmanaban, "Scenario-Based Planning of Participation of Virtual Power Plants in Storage and Energy Markets in Terms of Load Response and Market Price Uncertainty," *Journal of Green Energy Research and Innovation*, vol. 1, no. 3, pp. 77–95, 2024.

[26] B. Rostami, J. Ebrahimi, Z. Sabzian Molaee, V. Davatgaran, and S. A. Alavi, "Improving the Technical and Economic Indexes of Distribution Network by Three-Stage Enhanced Imperialist Competitive Algorithm," *Journal of Green Energy Research and Innovation*, vol. 1, no. 3, pp. 1–15, 2024.

[27] S. Darvish Kermani, M. Fayazi, J. Barati, and M. Joorabian, "Percentage of Islanding and Peninsulating Detection in Large Microgrids with Renewable Energy Resources with Multiple Connection Points to Different Grids," *Journal of Green Energy Research and Innovation*, vol. 1, no. 2, pp. 1–14, 2024.

[28] H. Makvandi, M. Abasi, et al., "Design of New Intelligent Islanding Detection Scheme in Multi-Machine Power Systems to Prevent Wide-Area Blackouts," *2022 12th Smart Grid Conference (SGC)*, pp. 1–7, 2022.

Declaration of competing interest

The authors declare that they have no known competing financial interests or personal relationships that could have appeared to influence the work reported in this paper. The ethical issues, including plagiarism, informed consent, misconduct, data fabrication and/or falsification, double publication and/or submission, redundancy, have been completely observed by the authors.

Bibliography

Mahyar Abasi was born in Iran, in 1989. He received the Ph.D. degree in electrical power engineering from Shahid Chamran University of Ahvaz, Ahvaz, Iran, in 2021. He is currently an Assistant Professor with the Electrical Engineering Department, Arak University, Arak, Iran. In 2021, he was introduced as the top researcher of Khuzestan Province, Iran. From 2021 to 2023, he successfully received four titles from the membership schemes of the National Elite Foundation in Iran. His research background is more than 60 published journal and conference papers, more than ten authored books, 11 industrial research projects, and a patent in power systems. His specialized interests are fault protection, detection, classification, and location in HVAC and HVDC transmission lines, control of reactive power and FACTS devices, evaluation and improvement of power quality, and power system studies.
Email: m-abasi@araku.ac.ir
ORCID: 0000-0001-5228-6803
Contribution Statement: Conceptualization, Data curation, Formal analysis, Investigation, Methodology, Resources, Software, Supervision, Roles/Writing - original draft, Writing-review & editing.

Ebrahim khanfari was born in 1989 in Iran. He received his bachelor's degree in Transmission Network Technology Engineering in 2017 from Khuzestan University of Applied Sciences, Faculty of Water and Electricity. He is currently a master's student in power engineering at Institute for Higher Education, ACECR, Khouzestan, Iran. His expertise is in the field of protection of power systems and FACTS devices.
Email: Aabrahim.khanfari@gmail.com
ORCID: 0009-0006-1969-0998
Contribution Statement: Formal analysis, Methodology, Software, Visualization.